# Theory of prospective tetrahedral perovskite ferroelectrics

Anindya Roy* and David Vanderbilt

*Department of Physics & Astronomy, Rutgers University, Piscataway, NJ 08854-8019, USA*

(Dated: December 23, 2010)

Using first-principles methods, we predict the energy landscape and ferroelectric states of double perovskites of the form $AA'BB'O_6$ in which the atoms on both the A and B sites are arranged in rock-salt order. While we are not aware of compounds that occur naturally in this structure, we argue that they might be realizable by directed synthesis. The high-symmetry structure formed by this arrangement belongs to the tetrahedral $F\bar{4}3m$ space group. If a ferroelectric instability occurs, the energy landscape will tend to have minima with the polarization along tetrahedral directions, leading to a rhombohedral phase, or along Cartesian directions, leading to an orthorhombic phase. We find that the latter scenario applies to $CaBaTiZrO_6$ and $KCaZrNbO_6$, which are weakly ferroelectric, and the former one applies to $PbSnTiZrO_6$, which is strongly ferroelectric. The results are modeled with a fourth- or fifth-order Landau-Devonshire expansion, providing good agreement with the first-principles calculations. Computations of zone-center soft modes are also carried out in order to characterize the polar and octahedral-rotation instabilities in more detail. Prospects for synthesis of ferroelectric materials belonging to this class are discussed.

## I. INTRODUCTION

Recent interest in novel materials has been stimulated by unprecedented advances both in experimental materials synthesis and in first-principles computational methods for predicting materials properties. Attention has focused in particular on functional materials that can be driven between various structural or electronic phases having distinct properties, as for example by the application of electric fields, magnetic fields, or strain.

Ferroelectric perovskites constitute a subset of these interesting compounds, with their switching behavior providing potential applications in non-volatile memories and their piezoelectric properties making them attractive as actuators and sensors. The perovskites are also of considerable interest in the search for multiferroics having strongly coupled polar and magnetic properties. Recent work has shown that many perovskite properties can be tuned through the application of epitaxial strain.[1–5]

Ferroelectric perovskite oxides can generally be classified into those derived from cubic symmetry, meaning that the actual or putative high-temperature symmetric phase is cubic, or those derived from tetragonal symmetry, meaning that the high-symmetry phase is tetragonal. Most well-known ferroelectrics, including $BaTiO_3$, $KNbO_3$, $PbTiO_3$, and $BiFeO_3$ belong to the first class, while some layered ferroelectrics, such as $SrBi_2Ta_2O_9$,[6–8] belong to the latter. It is possible for the compositional ordering in tetragonal layered systems to break inversion symmetry, as for example in "tricolor" superlattices.[9–12] To our knowledge, however, there are no perovskite oxides in which the chemical composition corresponds to a *tetrahedral* high-symmetry structure. While some boracites ($M_3B_7O_{13}X$, where M is usually a divalent metal and X is usually a halogen) such as $Ni_3B_7O_{13}I$ are realizations of this kind of tetrahedral ferroelectric system,[13–15] it would be very interesting to see the same symmetry class represented in the better-known cases of perovskite oxides.

The present work is motivated by the idea that perovskite oxides having a tetrahedral high-symmetry structure might be realized experimentally and might have interesting ferroelectric or other physical properties. With this in mind, we have carried out a computational study, based on first-principles density-functional calculations, of perovskites having a tetrahedral compositional symmetry. In particular, we focus on $AA'BB'O_6$ double perovskites in which both A and B sites exhibit rock-salt order. While rock-salt order on the B site of a double perovskite is common, it is quite rare on the A site, where a 50% mixing of two atoms typically leads to (001) layered ordering if it orders at all. Nevertheless, even if the tetrahedral symmetry is not realized in the equilibrium phase diagram, we shall argue that experimental routes to the directed synthesis of such double-rock-salt tetrahedral $AA'BB'O_6$ perovskites may be available.

The paper is organized as follows. Sec. II introduces the structure of the $AA'BB'O_6$ perovskite materials, describes the possible symmetry-determined directions of the polarization, and discusses possible domain types and their symmetries. We then briefly detail our theoretical methods in Sec. III. Sec. IV describes the results of our first-principles calculations and presents a comparison with a simple empirical model. We also discuss the effects of rotations of oxygen octahedra, and present some results concerning a Mn-containing double perovskite in which magnetic ordering is also an issue. Finally, in Sec. V we summarize our work and present our conclusions.
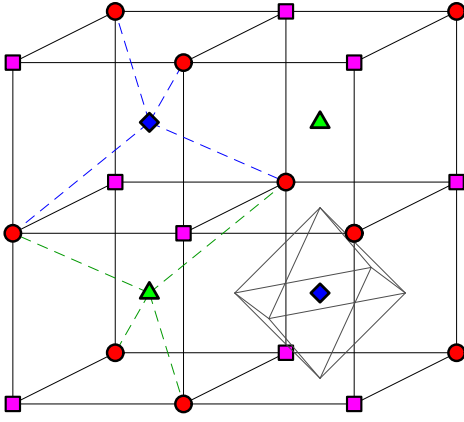
FIG. 1: (Color online) Structure of $AA'BB'O_6$ double perovskites, with A (red circles) and A$'$ (magenta squares) atoms forming one rock-salt framework, and B (blue diamonds) and B$'$ (green triangles) atoms forming a second interpenetrating one. Oxygen atoms are not shown, although one oxygen octahedron is outlined to clarify their role in the structure. Dashed lines illustrate the tetrahedral point symmetry.
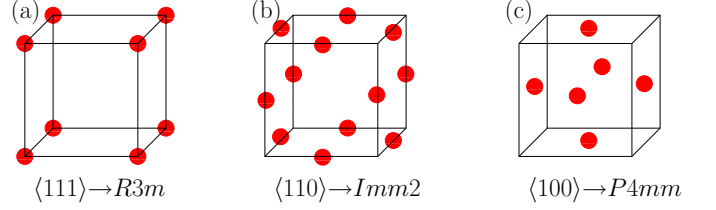
## II. TETRAHEDRAL $AA'BB'O_6$ DOUBLE PEROVSKITES WITH ROCK-SALT ORDER

We consider here a class of perovskite ferroelectrics whose compositional symmetry, and thus the high-temperature symmetric phase, is tetrahedral, instead of cubic or tetragonal. The simplest way to arrive at tetrahedral symmetry in the perovskite system is to populate both A and B sites with two different kinds of atoms (A and A$'$, and B and B$'$, respectively) arranged in rock-salt (three-dimensional checkerboard) order. The crystal chemistry of the perovskites, while preferring rock-salt ordering for B sites, resists the same on the A sites, where layered (001) ordering is preferred instead.[16,17] To our knowledge, no perovskite oxides exhibiting *simultaneous* A- and B-site rock-salt ordering has been reported. Nevertheless, we shall investigate their properties theoretically here.

The structure in question is illustrated in Fig. 1, in which oxygen atoms are suppressed for clarity. It can be seen that the point symmetry of each atom is tetrahedral, and since there is only one formula unit per primitive cell, this also establishes the crystal point group as tetrahedral, with the $F\bar{4}3m$ space group (216). This then identifies the parent high-symmetry structure, and can be compared with the $Pm3m$ high-symmetry structure that characterizes most ordinary perovskite ferroelectrics.

In such a tetrahedral ferroelectric, the symmetry of the energy landscape $E(\mathbf{P})$ is such that $E$ will be stationary with respect to the direction of $\mathbf{P}$ for $\mathbf{P}$ along $\langle 111 \rangle$, $\langle \bar{1}\bar{1}\bar{1} \rangle$, and $\langle 100 \rangle$ directions. If there are local minima along these directions, they correspond to the rhombohedral $R3m$ space group (160) in the first two cases, or the orthorhombic $Imm2$ space group (44) in the last case. This is illustrated in Fig. 2, where panels (a-c) il-
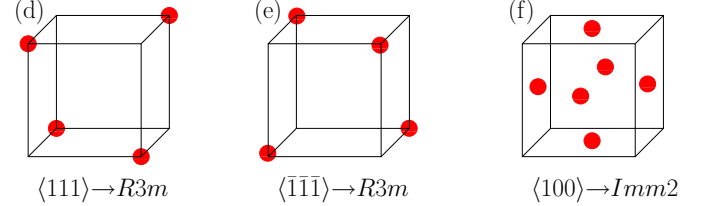
Cubic $Pm3m$ parent structure



FIG. 2: (Color online) Symmetry-determined possibilities for directions of energy minima in the space of polarization, represented by red dots. Fig. (a)-(c) cubic composition leading to high-symmetry $Pm3m$ structure, and (d)-(f) tetrahedral composition leading to high-symmetry $F\bar{4}3m$ structure.

lustrate the usual case of cubic perovskites, while panels (d-f) show the corresponding possibilities in the tetrahedral perovskite system. If the rhombohedral directions are energetically favored, as in panels (d-e), then there will be two distinct types of rhombohedral domains with different energies, and the dependence of the total energy on $P$ for $\mathbf{P} = P\hat{n}$ along the body diagonal $\hat{n}$ will display an asymmetric double-well potential. This is in sharp contrast with systems like $A_2BB'O_6$ or $AA'B_2O_6$, in which only one sublattice has rock-salt order; the symmetry is then that of panels (a-c), and the magnitude of the polarization does not change when the polarization is reversed during a domain switching event.

Even if these perovskites with double rock-salt do not exist as equilibrium phases, it may be possible to synthesize them using atomic-layer epitaxy techniques. In order to access the desired compositional order, this would need to be done by epitaxial growth on the (111) perovskite surface orientation. As a proof of principle, Rijnders, Blok and Blank have recently reported such a growth of $SrCaTiMnO_6$ and $CaBiTiFeO_6$ films on $LaAlO_3$ and $SrTiO_3$ substrates.[18] Interestingly, a symmetry analysis shows that a (111) uniaxial strain, of the kind that results from a lattice mismatch in this kind of epitaxial geometry, would convert the system to a polar space group by selecting out one of the body-diagonals as special, resulting in a polarization even when none is present in the high-symmetry tetrahedral structure. A related effect, in which improper ferroelectricity can be induced by octahedral rotations around a body-diagonal direction, will be discussed in Sec. IV D.

TABLE I: Compounds for which calculations have been carried out. Second column gives the acronym that we use to identify the compound. Lattice constants are calculated in the high-symmetry $F\bar{4}3m$ structure and are reported in terms of an effective 5-atom cubic cell dimension. "Average" refers to the average computed lattice constant of the $ABO_3$, $A'BO_3$, $AB'O_3$, and $A'B'O_3$ parent materials.

| Compound | Alias | Lattice constant (a.u.) | |
| --- | --- | --- | --- |
| | | Calculated | Average |
| $PbSnTiZrO_6$ | PSTZ | 7.47 | 7.47 |
| $KCaZrNbO_6$ | KCZN | 7.55 | 7.55 |
| $CaBaTiZrO_6$ | CBTZ | 7.54 | 7.53 |
| $KSrTiNbO_6$ | KSTN | 7.35 | 7.33 |
| $KBaTiNbO_6$ | KBTN | 7.47 | 7.48 |
| $SrCaTiMnO_6$ | SCTM | 7.15 | 7.20 |

## III. COMPUTATIONAL DETAILS

The calculations are performed using density-functional theory (DFT) as implemented in the ABINIT code package.[19–21] We use Ceperley-Alder[22,23] exchange-correlation in the Perdew-Wang[24] parameterization, and Troullier-Martin norm-conserving pseudopotentials constructed using the FHI98PP[25] code. A plane-wave cut-off of 70 Hartree is applied. The Brillouin zone of the 10-atom fcc cell is sampled by a $6 \times 6 \times 6$ Monkhorst-Pack[26] $k$-point mesh, while that for the 20-atom unit cell is $6 \times 6 \times 4$. (Energy differences between a low-symmetry and a high-symmetry structures are always computed using an identical cell and k-point mesh.) A stress threshold of $2 \times 10^{-2}$ GPa is used for cell relaxation, and forces on ions are converged below $2.5 \times 10^{-3}$ eV/Å. The electric polarization is calculated using the Berry-phase approach.[27] To avoid any potential confusion in the branch choice for the polarization of non-orthogonal unit cells, we also estimated the polarization using the computed Born effective charge tensors and atomic displacements, finding good agreement.

In addition to ground-state relaxation calculations, we also use density-functional perturbation theory to compute the frequencies of the zone-center phonon modes, as an aid in identifying polar or nonpolar (e.g., octahedral rotation) instabilities. To this end, the phonon frequencies at the $\Gamma$ point of the 10-atom cell (corresponding to both $\Gamma$ and $R$ points of a 5-atom cubic cell) were calculated, and the corresponding soft-mode eigenvectors were analyzed for any unstable modes having imaginary frequency. The plane-wave cutoff and other details were the same as for the ground-state calculations.

## IV. RESULTS

### A. High-symmetry states

As mentioned in Sec. I, rock-salt ordering is not a common form of ordering on the A site of mixed perovskites, and we are not aware of any naturally-occurring $AA'BB'O_6$ double perovskites that exhibit rock-salt ordering on both A and B sites. Therefore, our first step has been to carry out a theoretical search for potential candidate materials of this kind. Even if the double rock-salt ordering is not the ground-state equilibrium structure for a given material, it could be a candidate for attempts at directed experimental synthesis. Thus, we have carried out calculations for a variety of compounds, placing each in the high-symmetry $F\bar{4}3m$ structure and minimizing the energy with respect to the lattice constant. We look for materials that are insulating, and select possible candidates showing a range of ionic sizes, or combinations of cationic charges. For example, we consider combinations where both parent perovskites have +2 and +4 cations, or those with one parent perovskite having +1 and +5 cations while the other has +2 and +4 cations. This search led us to focus on the six candidate materials that are listed in Table I. The second column of this Table gives the alias by which each compound will be denoted in the remainder of the paper ("PSTZ" for $PbSnTiZrO_6$, etc.).

The third column of Table I presents our calculated lattice constants for the $AA'BB'O_6$ double perovskites. In order to put these in context, we also calculate the cell constants of all relevant parent perovskites in their high-symmetry $Pm3m$ structure. Then, for each of these six compounds, we average the calculated lattice constants of the four parent materials (even if some were occasionally metallic) and present the result as the last column of Table I. In each case we find that the cell constant of the double perovskite is very close to average of the parents. For PSTZ, for example, we find that the parents $PbTiO_3$, $PbZrO_3$, $SnTiO_3$ and $SnZrO_3$ have cell constants of 7.30, 7.70, 7.23 and 7.66 a.u. respectively. The corresponding arithmetic average is 7.47 a.u., essentially the same as the calculated value for PSTZ. The fact that the agreement is so good for all six cases indicates that the volumes of the parent simple perovskites essentially determine the cell constants of the double perovskites in the rock-salt structure. (Note that the results reported for SCTM are calculated in the high-symmetry ferromagnetic spin state, even though the antiferromagnetic structure is lower in energy; we do this to stay in the spirit of reporting the high-symmetry behavior here. More realistic spin structures will be considered in Sec. IV E.)

### B. Exploration of polar instabilities

Next we look for ferroelectric instabilities in these systems by checking the high-symmetry $F\bar{4}3m$ structures

TABLE II: Frequency and principal character of lowest zone-center mode, and same for next-higher mode, in the $F\bar{4}3m$ structure for AA′BB′O$_6$ materials.

| AA′BB′ | Phonon I | | Phonon II | |
|---|---|---|---|---|
| | $\omega$ (cm$^{-1}$) | char. | $\omega$ (cm$^{-1}$) | char. |
| PSTZ | $182i$ | O only | $160i$ | A′, O |
| KCZN | $195i$ | O only | $96i$ | A′, O |
| CBTZ | $147i$ | O only | $75i$ | A, O |
| KSTN | $103i$ | O only | | |
| KBTN | $149$ | A, A′, O | | |
| SCTM | $172i$ | O only | | |

to see if there are any phonon modes with imaginary frequency. Because of the high symmetry, all phonon modes at Γ have three-fold degeneracy. After identifying and discarding the triplet corresponding to the zero mode (uniform translation), we report the lowest relevant mode frequencies in the second and fourth columns of Table II. We also inspect the mode eigenvectors and report the character of these modes in the third and fifth columns of the Table.

We find that KBTN does not exhibit any unstable modes, suggesting that it is probably stable (or, at least, metastable) in the $F\bar{4}3m$ structure. Turning now to the other five materials, we see that there are *two* sets of unstable soft modes for the first three materials, while there is only one for KSTN and SCTM. Moreover, the most unstable mode always has character only on oxygen atoms, indicating that it corresponds to a pattern of octahedral tilts or rotations. Since this occurs at the Γ point of the 10-atom cell, it corresponds to an $R$-point instability of the 5-atom parent perovskite. (We shall consider rotational instabilities further in Sec. IV D.) However, if we look at the other set of unstable modes for each of the first three materials, we observe a large contribution coming from the smaller of the A ions, signaling that they are polar (i.e., infrared-active) distortions. We henceforth focus our attention on an in-depth study of the first three materials, namely CBTZ, KCZN and PSTZ.

As discussed in Sec. II, a ferroelectric distortion along one of the Cartesian directions leads to a polarized structure in the $Imm2$ space group, while the evolution of a polarization along the $\langle 111 \rangle$ or $\langle \bar{1}\bar{1}\bar{1} \rangle$ directions leads to the $R3m$ space group. For each material we follow the system into its local symmetry-constrained ground state for each type of distortion, and we also compute the electric polarization in this state using the Berry-phase method. (Polarizations found by multiplying computed $Z^*$ values times computed displacements differ only slightly from those calculated using the Berry-phase approach.) The results are presented in the first four columns of Table III, where the energies are reported relative to that of the high-symmetry $F\bar{4}3m$ structure. (Note that $\langle 111 \rangle$ denotes the direction from an A atom to a B neighbor, while $\langle \bar{1}\bar{1}\bar{1} \rangle$ points to a B′ neighbor.)

We see that for CBTZ and KCZN the $Imm2$ structure

is energetically preferred over the $R3m$ structures, and the polarizations are also larger for the $Imm2$ structure. In these materials, the energies and polarizations are also very similar for the structures distorted along $\langle 111 \rangle$ and $\langle \bar{1}\bar{1}\bar{1} \rangle$ directions. On the other hand, the PSTZ system behaves very differently. It is strongly polar, with the depth of the double-well potential, at 0.6-0.8 eV, being more than an order of magnitude larger than for the other two materials. Furthermore, the $R3m$ structure denoted as $\langle \bar{1}\bar{1}\bar{1} \rangle$ is now the favored structure, being significantly lower in energy than either the $\langle 111 \rangle$ $R3m$ structure or the $Imm2$ structure. This structure also has the largest polarization, at 0.837 C/m$^2$.

We thus see that AA′BB′O$_6$ double perovskites can have a rich variety of polar behaviors, ranging from ones that remain nonpolar like KBTN, to those that are weakly polar like CBTZ and KCZN, and finally to the case of the strongly polar PSTZ. In the next subsection we shall see how this diversity of behaviors can be captured in a simple analytical model.

Before doing so, we comment briefly on the nature of the ferroelectricity seen in these tetrahedral ferroelectrics. For this purpose, we have inspected the eigenvectors of the ferroelectric soft modes identified in Table II. Letting $\xi_\mu$ be the sum of squares of soft-mode eigenvector components corresponding to atoms of type $\mu$, expressed as percentages, we find $\boldsymbol{\xi} = (\xi_A, \xi_{A'}, \xi_B, \xi_{B'}, \xi_O) = (0.5, 45.7, 1.4, 2.1, 50.3)$ for PbSnTiZrO$_6$, $\boldsymbol{\xi} = (0.1, 72.8, 0.2, 0.6, 26.3)$ for KCaZrNbO$_6$, and $\boldsymbol{\xi} = (78.5, 0.5, 0.3, 0.6, 20.1)$ for CaBaTiZrO$_6$. In all three cases, the ferroelectricity is found to be A-site driven, with very little involvement of B cations. More specifically, it is associated with a displacement of the smaller of the the A-site cations, coupled with some oxygen motion. This seems reasonable in retrospect, since the lattice constant of the overall AA′BB′O$_6$ material will be expanded by the larger A atom, leaving a "rattling cage" environment for the smaller one.

## C. Theoretical modeling

The results of our first-principles calculations of the energies and polarizations of tetrahedral double perovskites can be modeled by expressing the energy as a polynomial in the components of the electric polarization, as in Landau-Devonshire theory. Symmetry considerations exclude certain terms in the expansion, which is then written as

$$
\begin{aligned}
E = {} & \alpha(P_x^2 + P_y^2 + P_z^2) + \gamma P_x P_y P_z + \\
& \beta(P_x^4 + P_y^4 + P_z^4) + \eta(P_x^2 P_y^2 + P_y^2 P_z^2 + P_z^2 P_x^2) + \\
& \xi P_x P_y P_z(P_x^2 + P_y^2 + P_z^2) + \mathcal{O}(P^6) + \cdots \quad (1)
\end{aligned}
$$

where the energy is measured relative to that of the high-symmetry $F\bar{4}3m$ space group. (Note that the $\gamma$ and $\xi$ terms would vanish according to cubic symmetry.) We

TABLE III: Calculated polarization and total-energy reduction (relative to the high-symmetry $F\bar{4}3m$ structure, per 10-atom cell) for distorted structures of CBTZ, KCZN, and PSTZ. Last four columns present results obtained from the models discussed in Sec. IV C (values in parentheses are exact by construction, as they were used as input to the fit).

| Material | Space group | *Ab-initio* results Polarization C/m$^2$ | Energy meV | Landau-Devonshire model Fourth order meV | % error | Fifth order meV | % error |
|---|---|---|---|---|---|---|---|
| CBTZ | $R3m\langle 111\rangle$ | 0.137 | 10.8 | 11.2 | 3 | (10.8) | (0) |
|  | $R3m\langle\bar{1}\bar{1}\bar{1}\rangle$ | 0.136 | 11.5 | 11.1 | 3 | 11.5 | 0 |
|  | $Imm2\langle 100\rangle$ | 0.163 | 16.0 | (16.0) | (0) | (16.0) | (0) |
| KCZN | $R3m\langle 111\rangle$ | 0.186 | 24.9 | 26.4 | 6 | (24.9) | (0) |
|  | $R3m\langle\bar{1}\bar{1}\bar{1}\rangle$ | 0.184 | 27.2 | 26.0 | 4 | 27.5 | 1 |
|  | $Imm2\langle 100\rangle$ | 0.219 | 36.6 | (36.6) | (0) | (36.6) | (0) |
| PSTZ | $R3m\langle 111\rangle$ | 0.777 | 681.4 | 713.1 | 5 | (681.4) | (0) |
|  | $R3m\langle\bar{1}\bar{1}\bar{1}\rangle$ | 0.837 | 794.0 | 799.6 | 1 | 839.5 | 6 |
|  | $Imm2\langle 100\rangle$ | 0.709 | 581.8 | (581.8) | (0) | (581.8) | (0) |

denote the energy and the polarization of the orthorhombic $Imm2$ space group by $E_{\langle 100\rangle}$ and $P_{\langle 100\rangle}$ respectively. For the rhombohedral space group $R3m$, we have correspondingly $E_{\langle 111\rangle}$, $P_{\langle 111\rangle}$, $E_{\langle\bar{1}\bar{1}\bar{1}\rangle}$ and $P_{\langle\bar{1}\bar{1}\bar{1}\rangle}$. $P_{\langle 111\rangle}$ and $P_{\langle\bar{1}\bar{1}\bar{1}\rangle}$ represent the positive and negative polarizations of the two minima along the body diagonals. For ordinary ferroelectric materials these polarization values are equal in magnitude, and so are their related energies. In the orthorhombic case we take the $z$ axis to be the symmetry axis, so that $P_x = P_y = 0$ and $P_z = P$. In the rhombohedral case we keep the Cartesian alignment of the axes, such that $P_x = P_y = P_z = P/\sqrt{3}$.

Thus, from our *ab-initio* calculations we have the calculated values of the six quantities $E_{\langle 111\rangle}$, $E_{\langle\bar{1}\bar{1}\bar{1}\rangle}$, $E_{\langle 100\rangle}$, $P_{\langle 111\rangle}$, $P_{\langle\bar{1}\bar{1}\bar{1}\rangle}$, and $P_{\langle 100\rangle}$ that we can use to determine the free parameters in Eq. (1). If we truncate Eq. (1) at fifth order as shown, we have six quantities to determine five parameters, thus overconstraining the solution. Similarly, if we truncate Eq. (1) at fourth order, we overconstrain more strongly (six constraints and four parameters). Going in the other direction to include sixth order in Eq. (1) would be problematic because several invariants appear at sixth order, so that more than six constraints would be needed to determine the system of equations. We therefore attempted the fits with the polynomial truncated at fourth and fifth order. When working at fourth order, we use all values except $E_{\langle 111\rangle}$ and $E_{\langle\bar{1}\bar{1}\bar{1}\rangle}$ in the fit, and then test whether we can successfully predict the values of these two quantities. At fifth order, we omit only $E_{\langle\bar{1}\bar{1}\bar{1}\rangle}$, and test this value from the fit.

The comparison of the fitted energies with those computed from the first-principles calculations are presented in Table III. Values that were included in the fit, and are therefore exact by construction, are shown in parentheses. We see that even the fourth-order fit gives encouraging agreement, with a worst-case deviation of about 6%. However, a closer inspection reveals a specific feature of the fourth-order calculation that is qualitatively incor-

rect, namely that the fitted values of $E_{\langle\bar{1}\bar{1}\bar{1}\rangle}$ are smaller than those of $E_{\langle 111\rangle}$ for CBTZ and KCZN, while the DFT calculations give the opposite trend. This relates to the fact that these two materials have an anomalous behavior in that the *lower* magnitude of polarization is associated with the *deeper* energy minimum when comparing the $E_{\langle 111\rangle}$ and $E_{\langle\bar{1}\bar{1}\bar{1}\rangle}$ distortions (PSTZ does not show this anomalous behavior). It turns out that the fourth-order theory does not have enough flexibility to reproduce this behavior; at that level of theory, it can be shown that $|\Delta E_{\langle 111\rangle}| > |\Delta E_{\langle\bar{1}\bar{1}\bar{1}\rangle}|$ if $|P_{\langle 111\rangle}| > |P_{\langle\bar{1}\bar{1}\bar{1}\rangle}|$, and vice versa. This discrepancy is removed once we go to the fifth-order theory; as can be seen from Table III, the relative magnitudes of the energies and polarizations are now correct for CBTZ and KCZN, and the discrepancy between the model predictions and *ab-initio* calculations improves substantially. Thus, we conclude that a fifth-order expansion is the minimum complexity needed to give a qualitatively correct description of the energy-polarization relations in the class of AA′BB′O$_6$ materials under study here. We note, however, that there are still quantitative errors for PSTZ; these can only be removed by going to still higher order, presumably because the larger magnitude of polarization in PSTZ accesses higher terms in the Landau-Devonshire expansion.

### D. Oxygen octahedral rotations

As we have seen in Table II, most of our investigated materials show unstable soft modes corresponding to tilts and rotations of the oxygen octahedra. In our investigation of the ferroelectric states in Sec. IV B, we neglected these modes by relaxing the systems according to symmetry constraints consistent with polar, but not rotational, instabilities. We now consider the effect of these rotations, which may compete with the ferroelectric distortions in determining the ground state of the system.

We use PSTZ as a test case for this purpose. As we saw

in Table II, PSTZ shows two unstable sets of modes in the high-symmetry $F\bar{4}3m$ structure, a rotational instability at $182\,i\,\mathrm{cm}^{-1}$ and a polar one at $160\,i\,\mathrm{cm}^{-1}$. If we follow the polar mode distortion into the polar $R3m\langle\bar{1}\bar{1}\bar{1}\rangle$ structure reported previously in Table III, we find that it is not a local energy minimum. Instead, we find that this structure still has an unstable phonon of frequency $22.7\,i\,\mathrm{cm}^{-1}$ corresponding to rotations of the octahedra about the polar $\langle\bar{1}\bar{1}\bar{1}\rangle$ axis (i.e., like an $R$-point mode of the ideal 5-atom perovskite structure). Turning on these rotations, the system reaches a stable $R3$ structure at small rotation angles of $\sim$0.46° and $\sim$0.79° around $\langle\bar{1}\bar{1}\bar{1}\rangle$ for the octahedral rotations centered on B and B′ atoms respectively. The phonon mode that was previously unstable is now found to have a positive frequency, while other low-lying mode frequencies and the electric polarization remain almost unchanged. This new phase is energetically approximately equal to the $R3m\langle\bar{1}\bar{1}\bar{1}\rangle$ state. Thus, we find that while the rotations are present in the ground state, they are small and have little influence on the properties of the system.

To check whether this structure is truly the global ground state, we tested what happens if we follow a different route, i.e., starting from the high-symmetry $F\bar{4}3m$ space group and following the path of the unstable octahedral rotation (mode frequency $182i$ in Table II) without intentionally making any polar distortion. However, because it singles out one of the four {111} axes that were previously equivalent, such a rotation immediately converts the system to the *polar* rhombohedral space group $R3$. Relaxation within this space group is then found to lead back to the same structure we found before, in which strong polar distortions predominate over small rotations. Thus, we again conclude that the rotations are unimportant for PSTZ.

While the calculations above are specific to PSTZ, the symmetry analysis is more general and hints at the possibility of obtaining polar samples even if the dominant unstable modes have rotational character. In fact, there is an interesting possibility that even if there are *no* unstable polar modes in the high-symmetry $F\bar{4}3m$ structure, an unstable rotational mode could take the system into a polar space group. This would correspond to the discovery of a new class of improper ferroelectrics, in which the primary order parameter is the antiferrodistortive rotation, but in which a polarization necessarily appears because the selection of a rotation axis in a parent structure without inversion symmetry results in secondary polar distortions along that rotation axis. Moreover, it is interesting that *electric* fields could, at least in principle, be used to control the selection of the *rotational* domains in such a material, at least as far as selecting one of the rotation axes from among the four possible ones.

We already have such cases at our disposal: both KSTN and SCTM have rotational soft modes at the high-symmetry phase, but no polar soft modes. In the case of KSTN, allowing rotation leads to an $R3$ phase which is about 30 meV lower in energy than the high-symmetry
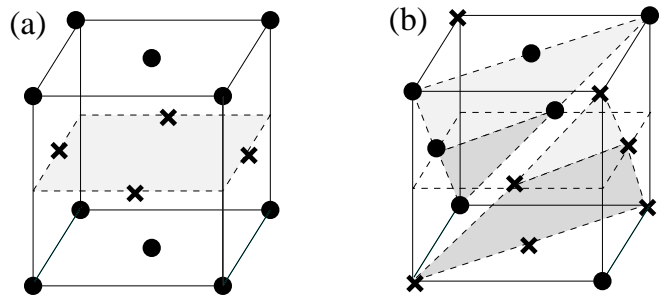


FIG. 3: (a) Type-I and (b) type-II configuration of SCTM.

structure, and has a polarization of 0.0023 C/m². This value of polarization is indeed tiny, about 1% of that seen in the KCZN case, which has a comparable energy difference between $R3m$ and $F\bar{4}3m$ phases. In the next section we discuss a similar behavior that emerges from our studies of SCTM.

## E. Magnetic SCTM structures

Recently, Rijnders, Blok and Blank[18] have succeeded in preparing films of the double perovskite SCTM in rock-salt order using layer-by-layer molecular-beam epitaxy on the (111) surface of LaAlO₃. To our knowledge, this is the first experimental realization of an AA′BB′ perovskite system in the double rock-salt arrangement. While their initial characterization of this material does not appear to show a polar character, we were motivated to extend our theoretical calculations to this material in order to make contact with the experiments. We present our results on SCTM in more detail in the present section.

The presence of the magnetic Mn ions makes this material distinct from the others studied so far. Since Sr and Ca are 2+ and Ti is 4+, we find Mn in its 4+ oxidation state. With its $d^3$ filling in an octahedral environment, this configuration is naturally compatible with a local spin state in which the majority $t_{2g}$ states are filled and other $d$ states are empty. To handle the magnetic nature of the Mn atom, we perform collinear spin-polarized calculations, neglecting the spin-orbit coupling. We consider both ferromagnetic (FM) and antiferromagnetic (AFM) spin arrangements. The Mn atoms reside on an FCC lattice, which is capable of exhibiting several AFM structures, all of which are frustrated to some degree.[28] We perform calculations on two of the most common AFM variants, the ones of type I and II illustrated in Fig. 3(a) and (b) respectively. The spins are aligned ferromagnetically in-plane and antiferromagnetically out-of-plane with respect to (001) planes in the type-I structure, and with respect to (111) planes in the type-II structure.

We first consider the FM spin structure, for which some results were also reported earlier in Tables I-II. The resulting material is found to be insulating with a re-

TABLE IV: Lattice constants, energy (relative to FM state per 20-atom unit cell) and fraction of parallel nearest-neighbor (NN) and next-nearest-neighbor (NNN) spins for three magnetic structures of $SrCaTiMnO_6$.

| Structure | Latt. const. (a.u.) | Energy (meV) | NN | NNN |
|---|---|---|---|---|
| FM | 7.15 | 0 | 12/12 | 6/6 |
| AFM (type-I) | 7.15 | −50 | 4/12 | 6/6 |
| AFM (type-II) | 7.15 | −70 | 6/12 | 0/6 |

laxed lattice constant of 7.15 a.u. in its high-symmetry structure. (It also shows a rotational instability which we have not pursued here.) However, both of the AFM structures considered are lower in energy, as shown in Table IV. The AFM arrangement of spins lowers the symmetry from $F\bar{4}3m$ to tetragonal $P\bar{4}m2$ and rhombohedral $R3m$ space groups for type I and II ordering, respectively. After relaxation, the new lattice constants still closely resemble that of the high-symmetry structure (e.g., the $c/a$ for the $p\bar{4}m2$ case is 0.9996). It is primarily the motion of the ions off the high-symmetry positions, brought about by the specific spin configurations, that defines the new space groups. Both these AFM cases are found to be insulators, with the type-II arrangement being slightly lower in energy. Table IV also provides a concise summary of the number of parallel nearest-neighbor and next-nearest-neighbor spins out of all such neighbors.

Next, we find the phonon frequencies at the $\Gamma$ point of this relaxed type-II AFM cell. There is one set of three soft modes, but the eigenmode analysis reveals them to be oxygen zone-boundary phonons, ruling out the possibility of a polar instability. This seems to be consistent with the experimental characterization of Rijnders *et al.*[18] However, instead of stopping here, we take the analysis a bit further, following the spirit of the last section on zone-boundary rotation of oxygen octahedra. Following the unstable mode in the $R3m$ phase, we arrive at the polar $R3$ space group, and find it to be lower than the $R3m$ phase by 319 meV (per 20-atom unit cell). As pointed out before, the $R3$ phase is a polar phase and exhibits an improper polarization induced by rotation of the oxygen octahedra. The calculated polarization is found to be very small, about 0.01 C/m$^2$, and points along the $\langle 111 \rangle$ direction. A phonon analysis in this phase reveals that two modes still remain soft, indicating that the ground state of the system has not yet been reached. We expect that further relaxation along these soft modes would lead

to a lower-symmetry structure with additional octahedral rotations, but still with a very small polarization.

While it lies beyond the scope of the present investigation, we note that it may also be of interest to consider the effects of epitaxial strain on the SCTM system. This could provide more direct contact with the experimental work on epitaxial growth mentioned earlier, as well as possibly making contact with recent work[5] showing that $SrMnO_3$, which is one of the parent perovskites of SCTM, can be driven between FM/FE and AFM/PE states via application of epitaxial strain. These considerations are left for future investigations.

## V. SUMMARY

In summary, we have carried out a first-principles study of the properties of prospective $AA'BB'O_6$ perovskites having double rock-salt order. We find several candidate compounds that are predicted to have ferroelectric instabilities associated with A-site displacements, with PSTZ ($PbSnTiZrO_6$) being of special interest because of its large spontaneous polarization and peculiar energy landscape having four global minima along $\langle \bar{1}\bar{1}\bar{1} \rangle$ directions and four secondary local minima along $\langle 111 \rangle$ directions. Compounds in this class may also be capable of exhibiting improper ferroelectricity based on rotation of oxygen octahedra, again stemming from the lack of inversion symmetry in the high-symmetry space group. We also predict that epitaxial strain can, under appropriate conditions, induce a polarization in an otherwise paraelectric material of this class. The inclusion of magnetic cations may provide interesting opportunities for the realization of novel magnetoelectric or multiferroic materials.

While initial attempts at the synthesis of such materials have not yet resulted in the demonstration of ferroelectricity, they do provide an existence proof that such synthesis is possible. We hope that the crossing of this hurdle will stimulate attempts at synthesis by other groups, and that eventual success will lead to novel ferroelectric materials having interesting and potentially useful physical properties.

### Acknowledgments

* Electronic address: anindya@physics.rutgers.edu

[1] K. M. Rabe, Current Opinion in Solid State and Materials Science **9**, 122 (2005).

[2] C. Ederer and N. A. Spaldin, Phys. Rev. Lett. **95**, 257601 (2005).

[3] O. Diéguez, K. M. Rabe, and D. Vanderbilt, Phys. Rev. B **72**, 144101 (2005).

[4] C. J. Fennie and K. M. Rabe, Phys. Rev. Lett. **97**, 267602

(2006).

[5] J. H. Lee and K. M. Rabe, Phys. Rev. Lett. **104**, 207204 (2010).

[6] M. G. Stachiotti, C. O. Rodriguez, C. Ambrosch-Draxl, and N. E. Christensen, Phys. Rev. B **61**, 14434 (2000).

[7] M.-H. Tsai, Y.-H. Tang, and S. K. Dey, Journal of Physics: Condensed Matter **15**, 7901 (2003).

[8] J. M. Perez-Mato, M. Aroyo, A. García, P. Blaha, K. Schwarz, J. Schweifer, and K. Parlinski, Phys. Rev. B **70**, 214111 (2004).

[9] N. Sai, B. Meyer, and D. Vanderbilt, Phys. Rev. Lett. **84**, 5636 (2000).

[10] M. P. Warusawithana, E. V. Colla, J. N. Eckstein, and M. B. Weissman, Phys. Rev. Lett. **90**, 036802 (2003).

[11] H. N. Lee, H. M. Christen, M. F. Chisholm, C. M. Rouleau, and D. H. Lowndes, Nature **433**, 395 (2005).

[12] X. Wu, M. Stengel, K. M. Rabe, and D. Vanderbilt, Phys. Rev. Lett. **101**, 087601 (2008).

[13] E. Ascher, H. Rieder, H. Schmid, and H. Stössel, J. Appl. Phys. **37**, 1404 (1966).

[14] H. Schmid, Physica Status Solidi (B) **37**, 209 (1970).

[15] R. J. Nelmes, Journal of Physics C: Solid State Physics **7**, 3840 (1974).

[16] M. C. Knapp and P. M. Woodward, Journal of Solid State Chemistry **179**, 1076 (2006).

[17] P. Davies, H. Wu, A. Borisevich, I. Molodetsky, and L. Far-ber (2008).

[18] G. Rijnders, J. Blok and D.H.A. Blank, Bull. Am. Phys. Soc., **55**, 2010, http://meetings.aps.org/link/-BAPS.2010.MAR.P24.10.

[19] X. Gonze, J. M. Beuken, R. Caracas, F. Detraux, M. Fuchs, G. M. Rignanese, L. Sindic, M. Verstraete, G. Zerah, F. Jollet, et al., Comput. Mater. Sci. **25**, 478 (2002).

[20] X. Gonze, G. Rignanese, M. Verstraete, J. Beuken, Y. Pouillon, R. Caracas, F. Jollet, M. Torrent, G. Zerah, M. Mikami, et al., Z. Kristall. **220**, 558 (2005).

[21] X. Gonze, B. Amadon, P.-M. Anglade, J.-M. Beuken, F. Bottin, P. Boulanger, F. Bruneval, D. Caliste, R. Caracas, M. Ct, et al., Comput. Phys. Commun. **180**, 2582 (2009).

[22] D. Ceperley, Phys. Rev. B **18**, 3126 (1978).

[23] D. M. Ceperley and B. J. Alder, Phys. Rev. Lett. **45**, 566 (1980).

[24] J. P. Perdew and Y. Wang, Phys. Rev. B **45**, 13244 (1992).

[25] M. S. M. Fuchs, Comput. Phys. Commun. **119**, 67 (1999).

[26] H. J. Monkhorst and J. D. Pack, Phys. Rev. B **13**, 5188 (1976).

[27] R. D. King-Smith and D. Vanderbilt, Phys. Rev. B **47**, 1651 (1993).

[28] M. K. Phani, J. L. Lebowitz, and M. H. Kalos, Phys. Rev. B **21**, 4027 (1980).